Efficient transfer of spatial intensity and phase information of arbitrary modes via four-wave mixing in an atomic vapor

Onkar N. Verma,* Ravi K. Pandey, and Raja R. Yadav
Department of Physics, University of Allahabad, Prayagraj-211002, Uttar Pradesh, India

Anjlee Patel
Kamla Nehru Institute of Technology (KNIT), Sultanpur-228118, Uttar Pradesh, India

(Received 25 June 2022; accepted 1 November 2022; published 22 November 2022)

We propose a scheme to transfer the spatial intensity as well as phase information encoded initially in the spatial profile of a weak probe field onto a newly generated Stokes field in a nonlinear process of four-wave mixing (FWM). The FWM process is explored in a gaseous medium consisting of atoms modeled as a three-level system in the Λ configuration. We found that different orders of Hermite-Gaussian and Laguerre-Gaussian modes carried by a probe beam are effectively transferred to a Stokes beam. Interestingly, the transferred intensity of the Stokes beam is a clone of the probe beam, whereas the phase profile is conjugate to the probe. The phase distribution of the transmitted modes at the exit of the medium is explored by superimposing them on a copropagating plane wave. Moreover, the parametric amplification due to the nonlinear process of FWM prevents any information loss due to linear absorption and permits us to work at high optical depths. We found a structural similarity between transferred images of about 99%, which provides clear evidence for the successful transfer of information in the FWM process.

DOI: 10.1103/PhysRevA.106.053713

I. INTRODUCTION

Spatial modulation of optical properties of a nonlinear medium in transverse directions via intense laser beams provides flexibility to control the diffraction and absorption of copropagating beams. This is made possible by choosing a suitable transverse structure of the strong laser beam [1–3]. A spatially nonuniform laser beam induces transverse variation in the optical response of the medium. This leads to inhomogeneity of the medium and is widely explored in controlling the diffraction and absorption of laser beams [4–6]. It has also been broadly used in the creation of spatial optical solitons [7,8], all-optical waveguiding or antiwaveguiding [9–12], focusing or defocusing [13–16], beam steering [17–20], and self-imaging [21,22] techniques. An all-optical imaging technique based on transverse modulation of electromagnetically induced transparency (EIT) has been predicted theoretically [23,24] and observed experimentally [25,26]. In quantum optics, EIT is a quantum coherence and interference effect in which absorption of a weak probe field is reduced significantly by the application of an extra-intense control field [6,27]. In these EIT-based imaging schemes, it is shown that intensity profiles of the control field are successfully transferred to the probe beam with appreciable spatial resolution. Bortman-Arbiv *et al.* [28,29] have suggested an optical imaging technique based on the four-wave mixing (FWM) process in a two-level atomic system. They have shown that only the intensity profiles of a Gaussian and Laguerre-Gaussian (LG) mode of a pump beam can be cloned onto a weak probe beam and newly born FWM beam in waveguiding and antiwaveguiding configurations, respectively.

However, in all the above nonlinear imaging schemes, there is no discussion of the transfer of phase information between laser beams, and the schemes are restricted to transferring some specific modes only [28,29]. In the case of EIT, the optical response of the medium depends on the absolute value of the control field amplitude, which makes it phase insensitive [23,24]. In addition, the transferred probe image in EIT suffers strong absorption due to breaking of the two-photon resonance condition. This imposes a further limitation on the transfer of high-contrast images. In nonlinear optics, the method of four-wave mixing (FWM) is an intensity-dependent and phase-sensitive process where two (three) frequencies mutually interact to produce two (one) new frequencies [30]. The newly generated wave may be a phase conjugate to an input beam if FWM is degenerate in the sense that all four interacting waves have the same frequency. Moreover, the efficiency of the process is strongly dependent on phase-matching conditions.

Nonlinear FWM in both cold and hot atomic vapors has been explored widely due to its broad applications in optical phase conjugation [31–33], parametric amplification [34], frequency conversion [35–37], storage and retrieval of light pulses with uniform and nonuniform spatial profiles [38–40], generation of squeezed light [41], and entangled photon pairs [42–45]. Braje *et al.* have reported the first experimental demonstration of efficient nonlinear frequency mixing using EIT at low light intensities [46]. Walker *et al.* have reported the transfer orbital angular momentum (OAM) states of an

*onkarnath15verma@gmail.com

LG beam from near infrared pump light to blue light via FWM process is rubidium vapor [47]. Souto Ribeiro and co-workers have theoretically proposed and experimentally observed the transfer of images and phase conjugation in the process of stimulated parametric downconversion [48,49]. Recently, Hamedi *et al.* have discussed the transfer of optical vortices between laser pulses in an atomic vapor [50].

In this paper, we plan to study an efficient transfer of phase information along with spatial intensity of structured beams such as a Hermite-Gaussian (HG) or Laguerre-Gaussian (LG) probe beam to a newly generated Stokes beam via FWM in the presence of two strong control fields. It should be noted that the newly born Stokes beam has a slightly different frequency than the externally applied fields and such conversion is often required for technologies operating at different resonant frequencies. Furthermore, the gain due to parametric amplification compensates any absorption loss of the weak probe and Stokes beams at the expense of absorption in strong control fields [34].

The spatial distribution of phase profiles of the transmitted modes in a FWM process can be obtained by interfering these modes with a copropagating plane wave. Several experimental techniques based on Fabry-Pérot and Mach-Zehnder interferometers have been developed to observe the transverse phase profile of spatially structured laser beams [51–54]. Optical vortex beams such as the LG beam have a spatially varying phase profile and zero intensity on the beam axis [55,56]. The spiral phase of an LG beam gives rise to orbital angular momentum and is especially important when dealing with phase-dependent effects [57]. The interaction of such structured beams with nonlinear media may enable potential applications in optical tweezing [58], optical trapping, and storage of phase information in optical media [59].

This paper is organized as follows. In Sec. II A, we introduce our theoretical model for FWM in the Λ system. In Sec. II B, we employ a semiclassical theory to describe the dynamics of the atomic system and obtain analytical expressions for linear and nonlinear polarizations to the probe and Stokes fields. In Sec. II C, we derive the propagation equations for probe and Stokes fields under slowly varying envelope approximations. In Sec. III, we discuss our important results. In Sec. III A, we first assign the HG transverse profile for the probe field and then present our numerical results for transfer of spatial intensity and phase profiles to the frequency-converted Stokes field in the FWM process. In Sec. III B, we discuss our numerical results for the spatial intensity and phase transformation of different orders of an optical vortex beam. In Sec. III C, we calculate the fidelities between the transmitted images of probe and Stokes fields. Section IV provides a brief summary of the presented work.

II. THEORETICAL MODEL

A. Model system

We consider a cold homogeneous cloud of ^{87}Rb atoms modeled as a three-level system in the Λ configuration shown in Fig. 1. In an ordinary EIT system a weak probe field and a relatively strong control field couple to $|1\rangle \leftrightarrow |3\rangle$ and $|2\rangle \leftrightarrow |3\rangle$ transitions, respectively [6]. It should be noted

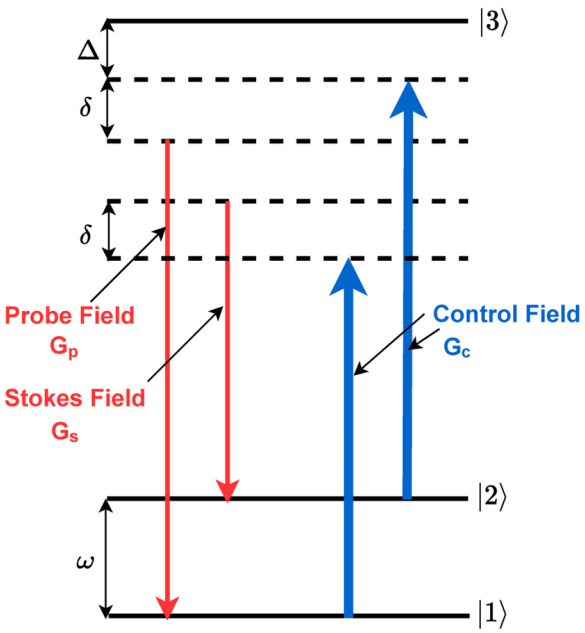

FIG. 1. Four-wave mixing in a three-level Λ-type atomic system. The Rabi frequencies of fields are denoted by G_j with $j \in \{p, c, s\}$. The single- and two-photon detunings are designated by Δ and δ, respectively. The ground-state frequency splitting is denoted by ω.

that EIT consideration is true for media with dilute atomic gases; for dense atomic media, stimulated Raman scattering is dominant, and an additional optical field is generated as the Stokes component [60,61]. However, EIT and Raman scattering processes are nonparametric in nature, and the phase-matching condition is not required for such processes. In the following, we use the parametric FWM process under the phase-matching condition to discuss the exchange of spatial information between laser beams. In the presence of stronger fields in resonant dense atomic media, the higher orders of polarization response become relevant, and this also results in the generation of new frequency components (Stokes and anti-Stokes) different from those applied fields [30,34]. So we take into account the additional interactions where the Stokes field operates at the $|2\rangle \leftrightarrow |3\rangle$ transition and the control field operates at the $|1\rangle \leftrightarrow |3\rangle$ transition (see Fig. 1). The three copropagating fields are defined as

$$\mathbf{E}_j(\mathbf{r}, t) = \mathbf{e}_j \mathcal{E}_j(\mathbf{r})\, e^{-i(\omega_j t - k_j z)} + \text{c.c.}, \tag{1}$$

where $\mathcal{E}_j(\mathbf{r})$ are the slowing varying envelope functions, $\mathbf{e}_j$ are the unit polarization vectors, ω_i are the laser field frequencies, and k_j are the wave numbers of fields. The subscripts $j \in \{p, c, s\}$ denote the probe, control, and Stokes fields. The frequency of the newly generated Stokes wave is $\omega_s = \omega_c - \omega$, provided that the two-photon resonance condition is satisfied. Here, ω is the frequency of the ground-state splitting.

The Hamiltonian of the atom-field system in the electric dipole and rotating wave approximation is given by

$$\begin{aligned}\hat{H} &= \hbar\omega_1|1\rangle\langle 1| + \hbar\omega_2|2\rangle\langle 2| + \hbar\omega_3|3\rangle\langle 3| \\ &\quad - \hbar(G_p e^{-i\omega_p t} + G_c e^{-i\omega_c t})|3\rangle\langle 1| \\ &\quad - \hbar(G_s e^{-i\omega_s t} + G_c e^{-i\omega_c t})|3\rangle\langle 2| + \text{H.c.},\end{aligned} \tag{2}$$

where $\hbar\omega_j$ is the energy of the corresponding atomic states $|j\rangle$. The parameters $G_p = \mathbf{d}_{31}\cdot\mathbf{e}_p\mathcal{E}_p e^{ik_p z}/\hbar$, $G_c = \mathbf{d}_{32}\cdot\mathbf{e}_c\mathcal{E}_c e^{ik_c z}/\hbar$, and $G_s = \mathbf{d}_{32}\cdot\mathbf{e}_s\mathcal{E}_s e^{ik_s z}/\hbar$ are referred to as Rabi frequencies of the probe, control, and Stokes fields, respectively. Here, $\mathbf{d}_{jk}$ are the dipole moments of respective transitions $|j\rangle \leftrightarrow \langle k|$ and assumed to be the same for the two optical transitions.

B. Equation of motion

The master equation for the density operator ρ is given by

$$\dot{\rho} = -\frac{i}{\hbar}[\hat{H}, \rho] + \mathcal{L}_\gamma \rho. \tag{3}$$

The last term in Eq. (3) describes incoherent processes such as spontaneous emission and is determined by

$$\begin{aligned}\mathcal{L}_\gamma[\rho] = &-\gamma_1(|3\rangle\langle 3|\rho - 2|1\rangle\langle 1|\rho_{33} + \rho|3\rangle\langle 3|)\\ &-\gamma_2(|3\rangle\langle 3|\rho - 2|2\rangle\langle 2|\rho_{33} + \rho|3\rangle\langle 3|)\\ &-\gamma_c(|2\rangle\langle 2|\rho - 2|1\rangle\langle 1|\rho_{22} + \rho|2\rangle\langle 2|)\\ &-\gamma_c(|1\rangle\langle 1|\rho - 2|2\rangle\langle 2|\rho_{11} + \rho|1\rangle\langle 1|).\end{aligned} \tag{4}$$

We label the radiative decay rate from state $|3\rangle$ to ground state $|j\rangle$ by $2\gamma_j$. Plugging the Hamiltonian of Eq. (2) into the master equation, we get the following equations of motion for the density matrix elements:

$$\begin{aligned}\dot{\rho}_{11} &= 2\gamma_2\rho_{33} - 2\gamma_c(\rho_{11}-\rho_{22}) + i(G_p^* e^{i\omega_p t} + G_c^* e^{i\omega_c t})\rho_{31}\\ &\quad -i(G_p e^{-i\omega_p t} + G_c e^{-i\omega_c t})\rho_{13}, \qquad (5a)\\ \dot{\rho}_{21} &= -[2\gamma_c + i\omega_{21}]\rho_{21} + i(G_s^* e^{i\omega_s t} + G_c^* e^{i\omega_c t})\rho_{31}\\ &\quad - i(G_p e^{-i\omega_p t} + G_c e^{-i\omega_c t})\rho_{23}, \qquad (5b)\\ \dot{\rho}_{22} &= 2\gamma_2\rho_{33} - 2\gamma_c(\rho_{22}-\rho_{11}) + i(G_s^* e^{i\omega_s t} + G_c^* e^{i\omega_c t})\rho_{32}\\ &\quad - i(G_s e^{-i\omega_s t} + G_c e^{-i\omega_c t})\rho_{23}, \qquad (5c)\\ \dot{\rho}_{31} &= -(\gamma_1+\gamma_2)\rho_{31} + i(G_s e^{-i\omega_s t} + G_c e^{-i\omega_c t})\rho_{21}\\ &\quad + i(G_p e^{-i\omega_p t} + G_c e^{-i\omega_c t})(\rho_{11}-\rho_{33}) - i\omega_{31}\rho_{31}, \qquad (5d)\\ \dot{\rho}_{32} &= -(\gamma_1+\gamma_2)\rho_{32} + i(G_p e^{-i\omega_p t} + G_c e^{-i\omega_c t})\rho_{12}\\ &\quad + i(G_s e^{-i\omega_s t} + G_c e^{-i\omega_c t})(\rho_{22}-\rho_{33}) - i\omega_{32}\rho_{32}, \qquad (5e)\\ \dot{\rho}_{33} &= -2(\gamma_1+\gamma_2)\rho_{33} + i(G_p e^{-i\omega_p t} + G_c e^{-i\omega_c t})\rho_{13}\\ &\quad - i(G_p^* e^{i\omega_p t} + G_c^* e^{i\omega_c t})\rho_{31}\\ &\quad + i(G_s e^{-i\omega_s t} + G_c e^{-i\omega_c t})\rho_{23}\\ &\quad - i(G_s^* e^{i\omega_s t} + G_c^* e^{i\omega_c t})\rho_{32}, \qquad (5f)\end{aligned}$$

where $\omega_{21} = \omega_2 - \omega_1$, $\omega_{31} = \omega_3 - \omega_1$, and $\omega_{32} = \omega_3 - \omega_2$. Now in order to solve the above equations analytically, we remove the time dependence by introducing suitable transformations given in Appendix A. So we find out perturbative solutions of the resulting density matrix equations (A2a)–(A2h) under the steady-state limit $\dot{\sigma} = 0$. For this, we assume that the probe and Stokes fields are weak enough in comparison to control fields and can be treated as a perturbation to the system in linear order. Thus the atomic coherences σ_{31} and σ'_{32} to first order in the probe and Stokes fields, and to all orders in the control field, are given by

$$\sigma_{31} = \mathcal{A}_p G_p + \mathcal{B}_p G_s^*, \tag{6a}$$

$$\sigma'_{32} = \mathcal{A}_s G_s + \mathcal{B}_s G_p^*, \tag{6b}$$

respectively, where the coefficients $\mathcal{A}_i$ and $\mathcal{B}_i$ are listed in Appendix B. Using the above, we obtain the nonlinear polarizations for the probe ($\mathbf{P}_p$) and Stokes ($\mathbf{P}_s$) fields:

$$\mathbf{P}_p = \mathcal{N}(\mathbf{d}_{31}\sigma_{31}e^{-i\omega_p t} + \text{c.c.}), \tag{7a}$$

$$\mathbf{P}_s = \mathcal{N}(\mathbf{d}_{32}\sigma'_{32}e^{-i\omega_s t} + \text{c.c.}), \tag{7b}$$

where $\mathcal{N}$ is the atomic density of the optical medium. These polarizations can also be expressed in terms of complex susceptibilities χ_{ij} of the atomic medium as follows:

$$P_p(\omega_p) = \chi_{11}\mathcal{E}_p + \chi_{12}e^{-i\Delta kz}\mathcal{E}_s^*, \tag{8a}$$

$$P_s(\omega_s) = \chi_{22}\mathcal{E}_s + \chi_{21}e^{-i\Delta kz}\mathcal{E}_p^*, \tag{8b}$$

where Δk is the projection of the geometric phase mismatch $\Delta\mathbf{k} = 2\mathbf{k_c} - \mathbf{k_p} - \mathbf{k_s}$ along the z axis, χ_{ii} ($\propto \mathcal{A}_{p,s}$) describe the linear susceptibilities for the probe and Stokes fields, and χ_{ij} ($\propto \mathcal{B}_{p,s}, i \neq j$) represents χ^3-type nonlinear susceptibilities responsible for the FWM process. The real part of χ_{ii} is related to an index of refraction which modifies the linear dispersion relation thereby influencing the phase-matching condition. The imaginary part of χ_{ii} is responsible for absorption of light fields. The nonlinear contribution acts as a source term in the propagation equations and enables efficient energy transfer between light fields provided that the phase-matching condition is satisfied ($\Delta\mathbf{k} = 0$).

It is evident from Eq. (8b) that even if the Stokes field is zero ($\mathcal{E}_s = 0$) at the entrance of the medium, there exists the nonlinear polarization of frequency ω_s, i.e.,

$$P_s(\omega_s) = \chi_{21}\mathcal{E}_p^*, \tag{9}$$

where we have assumed $\Delta\mathbf{k} = 0$. This simply implies that there is generation of a Stokes field at the output of the medium due to nonlinear interaction of the optical fields. Furthermore, it is interesting to note here that the polarization $P_s(\omega_s)$ is proportional to the complex conjugate of the probe ($\mathcal{E}_p^*$) and thus the generated Stokes wave would be a phase conjugate to the probe beam.

C. Beam propagation equations

We assume that the control fields are so strong that they are undepleted during propagation and merely acquire phase shifts due to self-phase modulation in the FWM process [30]. Thus we study only the effect of both linear and nonlinear contributions on the spatial evolution of the probe and the Stokes beams through the medium. In order to derive analytical expressions for beam propagation, we use Maxwell's wave equations:

$$\left(\nabla^2 - \frac{1}{c^2}\frac{\partial^2}{\partial t^2}\right)\mathbf{E}_j = \frac{4\pi}{c^2}\frac{\partial^2\mathbf{P}_j}{\partial t^2}, \tag{10}$$

where $\mathbf{P}_j$ are the macroscopic polarizations induced by the probe and Stokes fields. Using polarization expressions of Eqs. (7a) and (7b), the paraxial wave equations for the Rabi

frequencies of two fields assuming slowly varying envelopes in the z direction can be written as

$$\frac{\partial G_p}{\partial z} = \frac{i}{2k_p}\left(\frac{\partial^2}{\partial x^2} + \frac{\partial^2}{\partial y^2}\right)G_p + i\eta\sigma_{31}, \tag{11a}$$

$$\frac{\partial G_s}{\partial z} = \frac{i}{2k_s}\left(\frac{\partial^2}{\partial x^2} + \frac{\partial^2}{\partial y^2}\right)G_s + i\eta\sigma'_{32}, \tag{11b}$$

where η $(= 3\mathcal{N}\lambda^2/8\pi)$ is known as the coupling constant. The first terms in the parentheses on the right-hand sides account for the diffraction. The second terms on the right-hand sides are responsible for the dispersion and absorption of both the control and probe beams. Note that the two propagation equations are coupled via atomic coherences σ_{31} and σ'_{32}. We define the intensity gains for the probe and Stokes beams as $I_p = |G_p|^2/|G_{p0}|^2$ and $I_s = |G_s|^2/|G_{p0}|^2$, respectively. Here, G_{p0} is the seed signal on the input of the probe.

III. RESULTS AND DISCUSSION

We numerically simulate coupled equations (11a) and (11b) for different transverse modes of the probe beam and show how phase and intensity information is efficiently transferred to the newly generated Stokes beam.

A. Hermite-Gaussian mode

In order to interpret the efficient transfer of phase information, we first choose the transverse profile of the probe beam as a Hermite-Gaussian (HG) mode propagating along the z axis:

$$G_p(x, y, z) = G_{p0}\left(\frac{w_0}{w_z}\right) H_m\left(\frac{\sqrt{2}x}{w_z}\right)H_n\left(\frac{\sqrt{2}y}{w_z}\right) \times \exp\left[-\frac{r^2}{w_z^2} + \frac{ikr^2}{2R_z} - i\Phi_z\right], \tag{12}$$

where $r = \sqrt{x^2 + y^2}$ and the constants G_{p0} and w_0 are the input amplitude and waist radius of the probe beam, respectively. The function $H_m(x)$ is the Hermite polynomial of order m. The beam indices m and n determine the number of nodal lines along the x and y directions, respectively. The parameter w_z $(= w_p[1 + z^2/z_R^2]^{1/2})$ is the radius of the beam spot at position z at which the field amplitudes drop to $1/e$ of their axial values, and R_z $(= z + z_R^2/z)$ is the radius of curvature of the beam's wave fronts; z_R $(= \pi w_p^2/\lambda)$ is known as the Rayleigh range. The phase factor $\Phi_z = (m + n + 1)\psi_z$ is known as Gouy phase and describes an additional phase shift for a focused beam. Here, ψ_z $(= \tan^{-1}[z/z_R])$ is the Gouy phase shift for the fundamental Gaussian mode $(m = n = 0)$. The parameters w_z and R_z are independent of indices m and n, and thus all higher-order modes are described by the same functions.

For numerical simulations, we first consider an HG probe beam by setting indices $m = 1$, $n = 0$ in Eq. (12). The input amplitudes of the probe and control beams are set at $G_{p0} = 0.01\gamma$ and $G_{c0} = 1\gamma$. The initial waist size of the probe beam is fixed at $w_0 = 100\ \mu$m, which corresponds to a Rayleigh range about 4 cm from the waist. The input amplitude for the Stokes beam is taken to be zero at the entrance of the medium. In Fig. 2(a), we illustrate the spatial evolution of the transverse intensity gain profile of the probe as a function x at different propagation lengths of the 5-cm-long medium. During propagation over the initial few millimeters of distance, the probe is fully absorbed because the linear part dominates while the nonlinear part is negligible due to the zero-value Stokes field at $z = 0$. At a distance of about $z = 2$ cm the probe beam resumes its shape due to parametric amplification by the Stokes field. It is interesting to note that the probe is significantly amplified due to its coupling to a new beam created by FWM.

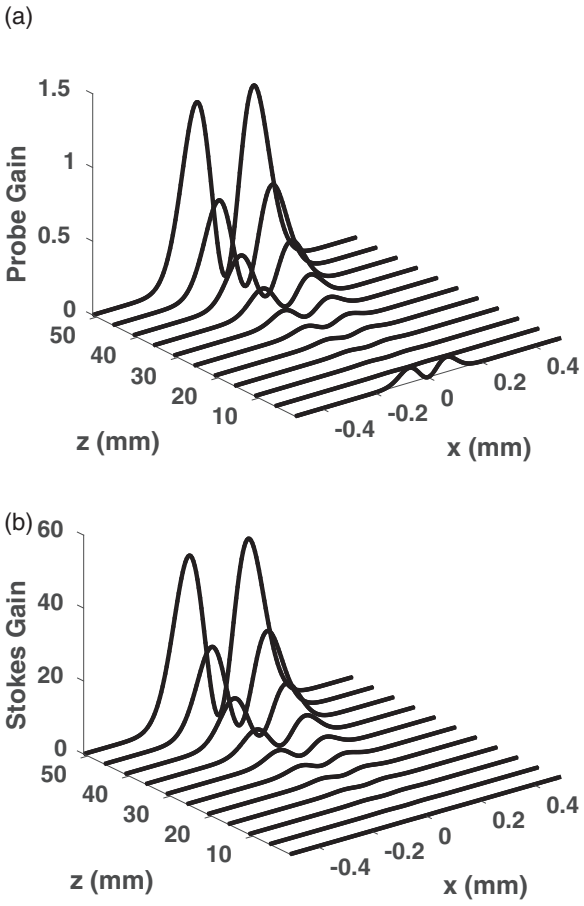

FIG. 2. The spatial evolution of the transverse intensity gain profile for (a) the probe beam and (b) the Stokes beam as a function of x at different propagation distances z. The parameters used are $G_p = 0.01\gamma$, $G_c = 1\gamma$, $\Delta = 0$, $\delta = 0$, $\gamma_0 = 0.01\gamma$, $\gamma = 9.4$ MHz, $\omega = 6.8$ GHz, $\lambda_p = 795$ nm, $w_0 = 100\ \mu$m, and $\mathcal{N} = 2\times10^{12}$ atoms/cm^3.

Figure 2(b) depicts the spatial evolution of the transverse intensity gain profile of Stokes beam as a function of x for various values of z. The Stokes field is zero at the input of the medium. After propagation of a few centimeters, the transverse structure of the probe is gradually mapped by the generated weak Stokes beam and amplified by parametric interaction. The integrated intensity gain for the probe is about 2, while for the Stokes beam it is nearly 75, at the output end of the medium. To compare the probe and Stokes beams at the output of the medium, we plot the cross-sectional intensity and phase profiles in Figs. 3(a) and 3(b) and Figs. 3(c) and

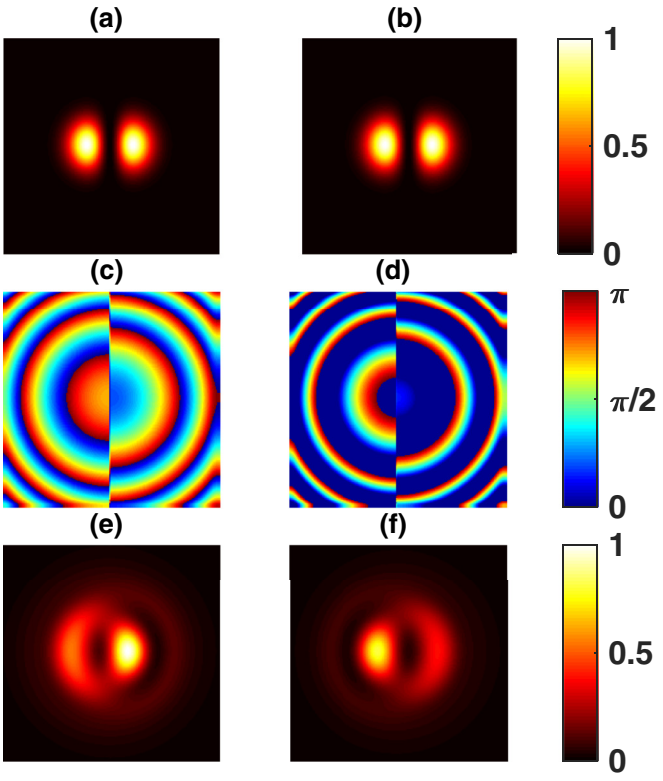

FIG. 3. Two-dimensional (2D) intensity distributions of the transmitted (a) probe and (b) Stokes beams in a plane transverse to the direction of propagation. The input probe beam indices are $m = 1,\ n = 0$; (c) and (d) show the corresponding phase profile, and (e) and (f) show the interference of these modes with a plane wave. All other parameters are the same as in Fig. 2.

3(d), respectively. The similarities between the 2D profiles of the two output beams clearly indicate that the effect of FWM is very efficient in this analysis. The transverse phase distribution of the output HG modes can be generated by the interference between output modes and a copropagating plane wave [51–54]. The interference patterns in Figs. 3(e) and 3(f) clearly show that the generated Stokes beam is a conjugate to the probe beam. A similar concept also applies to other higher-order spatial modes of the HG probe beam. In the following we choose a more complex structured light beam called an optical vortex.

B. Optical vortex mode

An optical vortex is basically a phase structured beam of the type $\exp(il\phi)$, where ϕ is the azimuthal angle and l is the azimuthal index and can be an integer. The phase in the field rotates about the propagation axis of the beam resulting in a helical wave front. This rotation of the phase structure of the vortex beam is the fundamental reason for the origin of the orbital angular momentum (OAM) of the light beam. The OAM can be either a negative integer or a positive integer depending on the direction of rotation. In addition, the transverse intensity profile of the vortex beam has a zero intensity at its center, thus forming a doughnut-shaped structure. A Laguerre-Gaussian (LG) mode has an optical vortex at its center, and we explore transferring its spiral phase profile from the probe beam onto the Stokes beam generated in the FWM process. For this, we choose the transverse profile of the probe beam as an LG mode of order (l, m):

$$G(r,\phi,z) = G_{p0}\sqrt{\frac{2m!}{\pi(m+|l|)}}\frac{w_p}{w_z}\left(\frac{\sqrt{2}r}{w_z}\right)^{|l|}L_m^{|l|}\left(\frac{2r^2}{w_z^2}\right) \times \exp\left[-\frac{r^2}{w_z^2}+\frac{ikr^2}{2R_z}\pm il\phi - i\Phi_z\right], \quad (13)$$

where $\Phi_z = (2m + |l| + 1)\psi_z$ is the Gouy phase shift. Here, m is the radial index, which is assumed to be zero for the present analysis. The functions $L_m^{|l|}(x)$ are the associated Laguerre polynomials. The input amplitude and waist radius of the probe beam are the same as before. For numerical simulations, we first use an LG structured probe beam of order $l = 1$. The spatial evolutions of the transverse intensity gain profile of the probe and Stokes beams are similar to those in Fig. 2. However, there is a significant change in the peak amplitude of the probe and Stokes gains by 0.2 and 7.5, respectively, at the end of the medium. As before, the transverse profile of the probe is initially absorbed due to the dominating effect of linear absorption. After a propagation distance of almost 2 cm, the probe beam gradually evolves and assumes its initial shape. The probe is enhanced by parametric amplification due to mutual coupling to the weak Stokes beam in the course of propagation. The input amplitude of the Stokes beam is again assigned a zero value at the entrance. However, due to the combined effects of linear and nonlinear terms induced by the control and probe beams, it rapidly evolves in the high-intensity region of the probe beam. The resulting Stokes profile has a doughnut-shaped structure with high intensity at its periphery. Thus an initially null field is generated due to FWM and shaped in such a way that its intensity profile is a replica of the probe beam. Moreover, the Stokes field is not only created but also amplified in the high-intensity region of the probe beam. The cross-sectional intensity distribution of the transmitted probe and Stokes beams at the output medium are shown in Figs. 4(a) and 4(b), and the corresponding phase profiles are depicted in Figs. 4(c) and 4(d). Again, the fact that the 2D profiles of the two output beams are identical reveals that the effect of the FWM process is very efficient. The output gain for both beams is approximately the same as before. In order to confirm the OAM of the vortex mode, the interference patterns of the superposition of output modes with a plane wave are illustrated in Figs. 4(e) and 4(f). This pattern contains a single spiral-shaped fringe steering out from the center [53,54]. Thus transverse phase information carried by an LG beam now is converted into an intensity distribution.

Since the OAM can also be a negative integer, we take azimuthal number $l = -2$ for further analysis. The results of the 2D intensity distribution of the transmitted probe and Stokes beams are shown in Figs. 5(a) and 5(b), respectively. It is clear that the LG probe profile is efficiently transferred to the Stokes field via the FWM process. However, the intensity distributions do not provide any information about the sign of the OAM. It is evident from Figs. 5(c) and 5(d) that the direction of the spiral phase structure is reversed in this case. The interference between the output LG modes and a

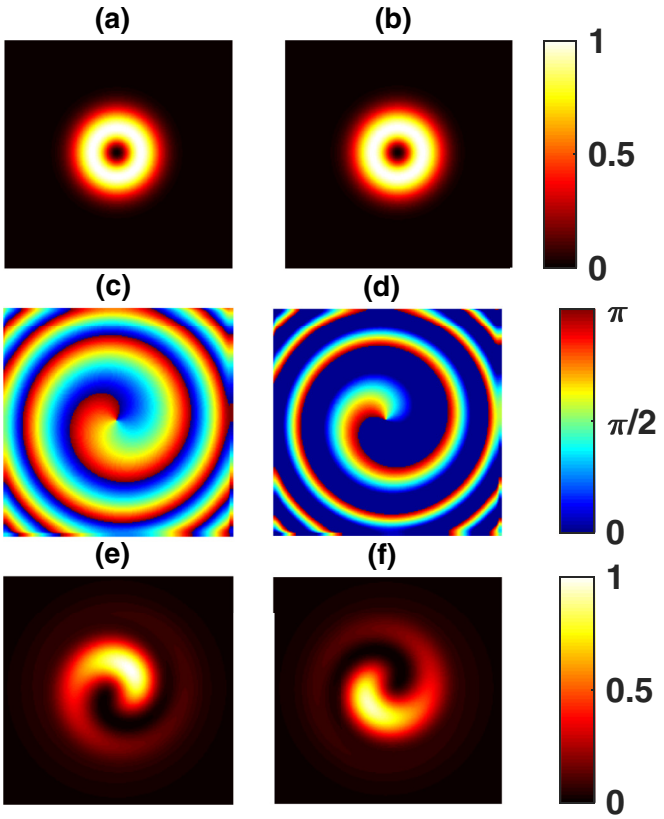

FIG. 4. 2D intensity distributions of the transmitted (a) probe and (b) Stokes beams in a plane normal to the direction of propagation. The input vortex probe beam has OAM $l = 1$; (c) and (d) show the corresponding helical phase patterns, and (e) and (f) show the interference of these modes with a plane wave.

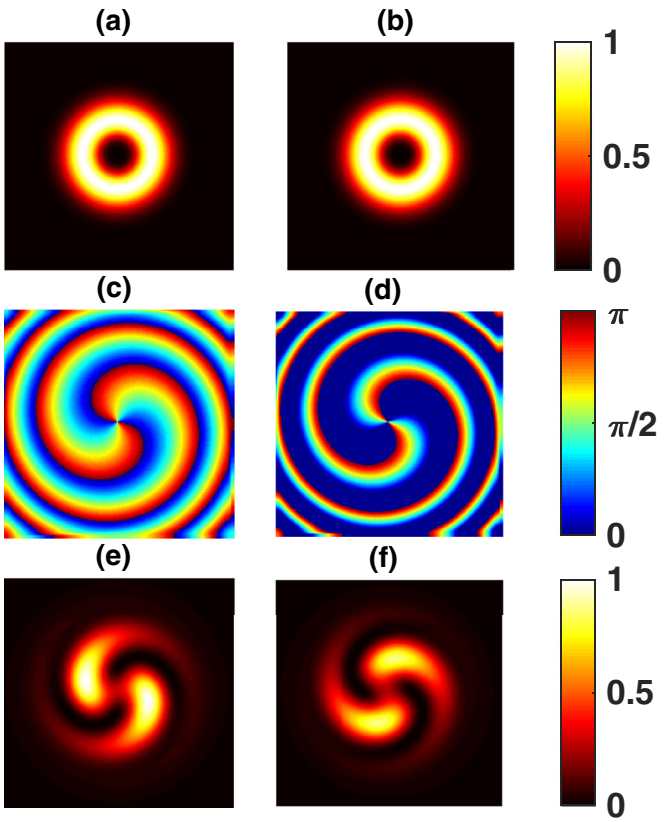

FIG. 5. 2D intensity distributions of the transmitted (a) probe and (b) Stokes beams in a plane normal to the direction of propagation. The input vortex probe beam has OAM $l = -2$; (c) and (d) show the corresponding helical phase patterns, and (e) and (f) show the interference of the output modes with a plane wave.

plane wave reveals the sign and OAM number information [see Figs. 5(e) and 5(f)] [53,54]. This time the interference pattern contains two spiral-shaped fringes fanning out from the center but in opposite direction as compared with positive l number. Therefore the OAM states with number $+l$ and $-l$ can also be identified in our study. We also observe a rotation of the interference fringes between two output modes. This is due to the relative phase change occurring between the linear and nonlinear parts of polarization. Note that a different OAM number l would correspond to a different bright spiral fringe. Therefore an LG mode with unknown l can be easily identified by counting the number of bright fringes. A similar concept also applies to other higher-order LG modes of the probe beam with positive azimuthal numbers. The present scheme of spatial phase transfer is also applicable to hypergeometric-Gaussian as well as Bessel-Gaussian modes.

C. Fidelity

The quality of transferred images can be measured by analyzing the fidelity. We find the fidelity between the transmitted probe and Stokes images by calculating the value of the structural similarity (SSIM) index, and to do this, the matrices corresponding to two images are compared using the MATLAB program [62]. A high value of the SSIM index indicates high fidelity between two images. The calculated similarities between two output images in the FWM process for different transverse modes of HG and LG laser beams are given in Table I. It is clear from Table I that there is a slight decrease in fidelities as we go to higher orders of transverse modes. This is due to a minute decrement in the gain intensities of the probe and Stokes beams. Interestingly, the similarity of about 99% clearly demonstrates a successful scheme of image transfer in the FWM process.

IV. CONCLUSION

We have theoretically suggested an efficient technique to transfer the spatial intensity as well as phase information of an arbitrary mode based on the FWM process in cold atomic ensembles. We have found that different orders of HG and LG modes encoded initially in the spatial envelope

TABLE I. Fidelities for various orders of HG and LG modes.

HG	Fidelity	LG	Fidelity
$m = 1,\ n = 0$	0.9976	$l = 1,\ m = 0$	0.9954
$m = 1,\ n = 1$	0.9964	$l = 2,\ m = 0$	0.9928
$m = 2,\ n = 0$	0.9962	$l = 3,\ m = 0$	0.9900
$m = 2,\ n = 1$	0.9948	$l = 4,\ m = 0$	0.9867
$m = 2,\ n = 2$	0.9930	$l = 5,\ m = 0$	0.9832

of a weak probe beam can be successfully transferred onto a newly generated Stokes field in a nonlinear process of FWM. Using the well-known interference technique, we have further shown that the phase distribution of transferred HG and LG modes over the Stokes beam is a phase conjugate to the output probe beam. We found that the Stokes beam not only transforms into a clone of the probe beam but also is amplified by parametric amplification. It is also observed that spatial overlap of the transverse profiles between two beams enhances mutual amplification during propagation. Moreover, the structural similarity between the transferred images of about 99% clearly indicates the success and efficiency of the optical FWM process.

ACKNOWLEDGMENTS

Discussions with Prof. Hari Prakash, Prof. Ranjana Prakash, Prof. Naresh Chandra and Ms. Shamiya Javed are gratefully acknowledged. O.N.V. gratefully acknowledges the financial support from the UGC, Government of India, for funding this research work through D.S. Kothari Postdoctoral Fellowship No. F.4-2/2006(BSR)/PH/20-21/0054.

APPENDIX A: ROTATING WAVE APPROXIMATION

The slowly varying envelopes are defined as

$$\rho_{ii} = \sigma_{ii}, \tag{A1a}$$

$$\rho_{31} = \sigma_{31}e^{-i\omega_p t} + \sigma'_{31}e^{-i\omega_c t}, \tag{A1b}$$

$$\rho_{32} = \sigma_{32}e^{-i\omega_c t} + \sigma'_{32}e^{-i\omega_s t}, \tag{A1c}$$

$$\rho_{21} = \sigma_{21}e^{-i(\omega_p-\omega_c)t}. \tag{A1d}$$

After substituting these in Eqs. (5a)–(5f), we make the rotating wave approximation. In doing this, we keep only the resonance terms and disregard the counter-rotating far-off resonance terms. Thus in a suitable interaction picture, the density matrix equations are expressed as

$$\dot{\sigma}_{11} = 2\gamma_2\sigma_{33} - 2\gamma_c(\sigma_{11}-\sigma_{22}) + iG_p^*\sigma_{31} - iG_p\sigma_{13} + iG_c^*\sigma'_{31} - iG_c\sigma'_{13}, \tag{A2a}$$

$$\dot{\sigma}_{21} = -\Gamma_{21}\sigma_{21} - iG_p^*\sigma_{23} - iG_c\sigma'_{23} + iG_c^*\sigma_{31} + iG_s^*\sigma'_{31}, \tag{A2b}$$

$$\dot{\sigma}_{22} = 2\gamma_2\sigma_{33} - 2\gamma_c(\sigma_{22}-\sigma_{11}) + iG_c^*\sigma_{32} - iG_c\sigma_{23} + iG_s^*\sigma'_{32} - iG_s\sigma'_{23}, \tag{A2c}$$

$$\dot{\sigma}_{31} = -\Gamma_{31}\sigma_{31} + iG_c\sigma_{21} + iG_p(\sigma_{11}-\sigma_{33}), \tag{A2d}$$

$$\dot{\sigma}'_{31} = -\Gamma'_{31}\sigma_{31} + iG_s\sigma_{21} + iG_c(\sigma_{11}-\sigma_{33}), \tag{A2e}$$

$$\dot{\sigma}_{32} = -\Gamma_{31}\sigma_{32} + iG_p\sigma_{12} + iG_c(\sigma_{22}-\sigma_{33}), \tag{A2f}$$

$$\dot{\sigma}'_{32} = -\Gamma'_{31}\sigma'_{32} + iG_c\sigma_{12} + iG_s(\sigma_{22}-\sigma_{33}), \tag{A2g}$$

$$\dot{\sigma}_{33} = -2(\gamma_1+\gamma_2)\sigma_{33} + iG_p\sigma_{13} - iG_p^*\sigma_{31} + iG_c\sigma'_{13} - iG_c^*\sigma'_{31} + iG_c\sigma_{23} - iG_c^*\sigma_{32} + iG_s\sigma'_{23} - iG_s^*\sigma'_{32}. \tag{A2h}$$

The rest of the equations can be found from $\dot{\sigma}_{ij} = \dot{\sigma}^*_{ji}$. The complex decay rates are defined as $\Gamma_{21} = 2\gamma_c + i\delta = \Gamma^*_{12}$, $\Gamma_{31} = [(\gamma_1+\gamma_2) + i(\Delta+\delta)] = \Gamma^*_{13}$, $\Gamma'_{31} = [(\gamma_1+\gamma_2) + i(\Delta+\omega)] = \Gamma'^*_{13}$, $\Gamma_{32} = [(\gamma_1+\gamma_2) + i\Delta] = \Gamma^*_{23}$, and $\Gamma'_{32} = [(\gamma_1+\gamma_2) + i(\Delta-\delta+\omega)] = \Gamma'^*_{23}$. Here, $\Delta = \omega_{32} - \omega_c$ and $\delta = \omega_{21} - (\omega_p - \omega_c)$ are the single- and two-photon detunings, respectively. Note that while deriving the above equations, we have imposed the condition $2\omega_c = \omega_p + \omega_s$, which signifies the energy conservation. In order to simplify the expressions, we have considered radiative decay rates $\gamma_1 = \gamma_2 = \gamma/2$ and $\gamma_c = \gamma_0/2$.

APPENDIX B: COEFFICIENTS FOR POLARIZATIONS

$$\mathcal{A}_p = i\frac{|G_c|^2\Gamma'_{31}(-N_{23}\Gamma'_{23} + N_{13}\Gamma_{23}) + N_{13}\Gamma'_{23}\Gamma'_{31}\Gamma_{21}\Gamma_{23}}{\Gamma'_{23}\Gamma'_{31}\Gamma_{21}\Gamma_{23}\Gamma_{31} + |G_c|^2\Gamma'_{31}\Gamma_{23}(\Gamma'_{23}+\Gamma_{31})}, \tag{B1}$$

$$\mathcal{B}_p = -i\frac{{G_c}^2(N_{13}\Gamma'_{23} + N_{23}\Gamma'_{31})\Gamma_{23}}{\Gamma'_{23}\Gamma'_{31}\Gamma_{21}\Gamma_{23}\Gamma_{31} + |G_c|^2\Gamma'_{31}\Gamma_{23}(\Gamma'_{23}+\Gamma_{31})}, \tag{B2}$$

$$\mathcal{A}_s = -i\frac{N_{23}\Gamma'_{13}\Gamma_{12}\Gamma_{13}\Gamma_{32} + |G_c|^2(N_{23}\Gamma'_{13} - N_{13}\Gamma_{13})\Gamma_{32}}{\Gamma'_{32}\Gamma'_{13}\Gamma_{12}\Gamma_{13}\Gamma_{32} + |G_c|^2\Gamma'_{13}\Gamma_{32}(\Gamma'_{32}+\Gamma_{13})}, \tag{B3}$$

$$\mathcal{B}_s = -i\frac{{G_c}^2(N_{23}\Gamma_{13} + N_{13}\Gamma_{32})\Gamma'_{13}}{\Gamma'_{32}\Gamma'_{13}\Gamma_{12}\Gamma_{13}\Gamma_{32} + |G_c|^2\Gamma'_{13}\Gamma_{32}(\Gamma'_{32}+\Gamma_{13})}, \tag{B4}$$

$$N_{13} = \rho_{11}^{(0)} - \rho_{33}^{(0)} = \frac{\gamma\Gamma'_{13}\Gamma'_{31}(2\gamma_0\Gamma_{23}\Gamma_{32} + |G_c|^2(\Gamma_{23}+\Gamma_{32}))}{D}, \tag{B5}$$

$$N_{23} = \rho_{22}^{(0)} - \rho_{33}^{(0)} = \frac{\gamma(2\gamma_0\Gamma'_{13}\Gamma'_{31} + |G_c|^2(\Gamma'_{13}+\Gamma'_{31}))\Gamma_{23}\Gamma_{32}}{D}, \tag{B6}$$

$$D = 4\gamma\gamma_0\Gamma'_{13}\Gamma'_{31}\Gamma_{23}\Gamma_{32} + 3|G_c|^4(\Gamma'_{13}+\Gamma'_{31})(\Gamma_{23}+\Gamma_{32}) + |G_c|^2(\gamma+3\gamma_0)[\Gamma'_{31}\Gamma_{23}\Gamma_{32} + \Gamma'_{13}(\Gamma'_{31}\Gamma_{23} + (\Gamma'_{31}+\Gamma_{23})\Gamma_{32})]. \tag{B7}$$

Note that the zeroth-order population differences N_{13} and N_{23} have been calculated in the absence of probe and Stokes fields.

[1] R. R. Moseley, S. Shepherd, D. J. Fulton, B. D. Sinclair, and M. H. Dunn, Phys. Rev. Lett. **74**, 670 (1995).

[2] R. R. Moseley, S. Shepherd, D. J. Fulton, B. D. Sinclair, and M. H. Dunn, Phys. Rev. A **53**, 408 (1996).

[3] A. Kasapi, M. Jain, G. Y. Yin, and S. E. Harris, Phys. Rev. Lett. **74**, 2447 (1995).

[4] D. D. Yavuz and N. A. Proite, Phys. Rev. A **76**, 041802(R) (2007).

[5] A. V. Gorshkov, L. Jiang, M. Greiner, P. Zoller, and M. D. Lukin, Phys. Rev. Lett. **100**, 093005 (2008).

[6] M. Fleischhauer, A. Imamoglu, and J. P. Marangos, Rev. Mod. Phys. **77**, 633 (2005).

[7] D. R. Walker, D. D. Yavuz, M. Y. Shverdin, G. Y. Yin, A. V. Sokolov, and S. E. Harris, Opt. Lett. **27**, 2094 (2002).

[8] N. A. Proite, B. E. Unks, J. T. Green, and D. D. Yavuz, Phys. Rev. A **77**, 023819 (2008).

[9] T. Hong, Phys. Rev. Lett. **90**, 183901 (2003).

[10] Y. V. Kartashov, V. A. Vysloukh, and L. Torner, Phys. Rev. Lett. **93**, 093904 (2004).

[11] D. Mihalache, D. Mazilu, F. Lederer, B. A. Malomed, Y. V. Kartashov, L.-C. Crasovan, and L. Torner, Phys. Rev. Lett. **95**, 023902 (2005).

[12] M. Mitsunaga, M. Yamashita, and H. Inoue, Phys. Rev. A **62**, 013817 (2000).

[13] B. B. Baizakov, B. A. Malomed, and M. Salerno, Phys. Rev. E **74**, 066615 (2006).

[14] A. G. Truscott, M. E. J. Friese, N. R. Heckenberg, and H. Rubinsztein-Dunlop, Phys. Rev. Lett. **82**, 1438 (1999).

[15] P. K. Vudyasetu, D. J. Starling, and J. C. Howell, Phys. Rev. Lett. **102**, 123602 (2009).

[16] R. Kapoor and G. S. Agarwal, Phys. Rev. A **61**, 053818 (2000).

[17] O. N. Verma and T. N. Dey, Phys. Rev. A **91**, 013820 (2015).

[18] Q. Sun, Y. V. Rostovtsev, and M. S. Zubairy, Phys. Rev. A **74**, 033819 (2006).

[19] V. A. Sautenkov, H. Li, Y. V. Rostovtsev, and M. O. Scully, Phys. Rev. A **81**, 063824 (2010).

[20] H. Wang and X. Peng, J. Opt. Soc. Am. B **29**, 429 (2012).

[21] J. Cheng and S. Han, Opt. Lett. **32**, 1162 (2007).

[22] F. Wang, C. Wang, J. Cheng, and D. Zhang, Appl. Opt. **53**, 1889 (2014).

[23] O. N. Verma, L. Zhang, J. Evers, and T. N. Dey, Phys. Rev. A **88**, 013810 (2013); O. N. Verma and S. Roy, Jpn. J. Appl. Phys. **57**, 08PF01 (2018).

[24] O. N. Verma and T. N. Dey, Phys. Rev. A **89**, 033830 (2014); O. N. Verma and S. Roy, IEEE J. Quantum Electron. **55**, 8200106 (2019).

[25] D. Ding, Z. Zhou, and B. Shi, Opt. Lett. **39**, 240 (2014).

[26] M. Cao, L. Zhang, Y. Yu, F. Ye, D. Wei, W. Guo, S. Zhang, H. Gao, and F. Li, Opt. Lett. **39**, 2723 (2014).

[27] S. E. Harris, Phys. Today **50**, 7, 36 (1997).

[28] D. Bortman-Arbiv, A. D. Wilson-Gordon, and H. Friedmann, Phys. Rev. A **63**, 031801(R) (2001).

[29] D. Bortman-Arbiv, A. D. Wilson-Gordon, and H. Friedmann, Opt. Commun. **204**, 371 (2002).

[30] R. W. Boyd, *Nonlinear Optics* (Academic Press, New York, 2008).

[31] A. Yariv and D. M. Pepper, Opt. Lett. **1**, 16 (1977).

[32] T.-Y. Fu and M. Sargent, Opt. Lett. **5**, 433 (1980).

[33] P. R. Hemmer, D. P. Katz, J. Donoghue, M. Cronin-Golomb, M. S. Shahriar, and P. Kumar, Opt. Lett. **20**, 982 (1995).

[34] M. D. Lukin, P. R. Hemmer, M. Loffler, and M. O. Scully, Phys. Rev. Lett. **81**, 2675 (1998).

[35] S. E. Harris, J. E. Field, and A. Imamoglu, Phys. Rev. Lett. **64**, 1107 (1990).

[36] M. Jain, H. Xia, G. Y. Yin, A. J. Merriam, and S. E. Harris, Phys. Rev. Lett. **77**, 4326 (1996).

[37] A. J. Merriam, S. J. Sharpe, M. Shverdin, D. Manuszak, G. Y. Yin, and S. E. Harris, Phys. Rev. Lett. **84**, 5308 (2000).

[38] R. M. Camacho, P. K. Vudyasetu, and J. C. Howell, Nat. Photon. **3**, 103 (2009).

[39] N. B. Phillips, A. V. Gorshkov, and I. Novikova, Phys. Rev. A **83**, 063823 (2011).

[40] J. Wu, Y. Liu, D.-S. Ding, Z.-Y. Zhou, B.-S. Shi, and G.-C. Guo, Phys. Rev. A **87**, 013845 (2013).

[41] R. E. Slusher, L. W. Hollberg, B. Yurke, J. C. Mertz, and J. F. Valley, Phys. Rev. Lett. **55**, 2409 (1985).

[42] C. H. van der Wal, M. D. Eisaman, A. André, R. L. Walsworth, D. F. Phillips, A. S. Zibrov, and M. D. Lukin, Science **301**, 196 (2003).

[43] Q.-F. Chen, B.-S. Shi, Y.-S. Zhang, and G.-C. Guo, Phys. Rev. A **78**, 053810 (2008).

[44] Q.-F. Chen, B.-S. Shi, M. Feng, Y.-S. Zhang, and G.-C. Guo, Opt. Express **16**, 21708 (2008).

[45] V. Boyer, A. M. Marino, and P. D. Lett, Phys. Rev. Lett. **100**, 143601 (2008).

[46] D. A. Braje, V. Balic, S. Goda, G. Y. Yin, and S. E. Harris, Phys. Rev. Lett. **93**, 183601 (2004).

[47] G. Walker, A. S. Arnold, and S. Franke-Arnold, Phys. Rev. Lett. **108**, 243601 (2012).

[48] P. H. Souto Ribeiro, S. Pádua, and C. H. Monken, Phys. Rev. A **60**, 5074 (1999).

[49] P. H. Souto Ribeiro, D. P. Caetano, M. P. Almeida, J. A. Huguenin, B. Coutinho dos Santos, and A. Z. Khoury, Phys. Rev. Lett. **87**, 133602 (2001).

[50] H. R. Hamedi, J. Ruseckas, E. Paspalakis, and G. Juzeliūnas, Phys. Rev. A **99**, 033812 (2019).

[51] V. Yu Bazhenov, M. V. Vasnetsov, and M. S. Soskin, JETP Lett. **52**, 429 (1990).

[52] N. R. Heckenberg, R. Mcduff, C. P. Smith, H. Rubinsztein-Dunlop, and M. J. Wegener, Opt. Quantum Electron. **24**, S951 (1992).

[53] M. Harris, C. A. Hill, and J. M. Vaughan, Opt. Commun. **106**, 161 (1994).

[54] M. Padgett, J. Arlt, N. Simpson, and L. Allen, Am. J. Phys. **64**, 77 (1996).

[55] L. Allen, M. W. Beijersbergen, R. J. C. Spreeuw, and J. P. Woerdman, Phys. Rev. A **45**, 8185 (1992).

[56] M. J. Padgett, Opt. Express **25**, 11265 (2017).

[57] A. M. Yao and M. J. Padgett, Adv. Opt. Photon. **3**, 161 (2011).

[58] H. He, M. E. J. Friese, N. R. Heckenberg, and H. Rubinsztein-Dunlop, Phys. Rev. Lett. **75**, 826 (1995).

[59] M. Padgett and R. Bowman, Nat. Photon. **5**, 343 (2011).

[60] K.-I. Harada, T. Kanbashi, M. Mitsunaga, and K. Motomura, Phys. Rev. A **73**, 013807 (2006).

[61] G. S. Agarwal, T. N. Dey, and D. J. Gauthier, Phys. Rev. A **74**, 043805 (2006).

[62] Z. Wang, A. C. Bovik, H. R. Sheikh, and E. P. Simoncelli, IEEE Trans. Image Process. **13**, 600 (2004).